Comparison of Numerical Solutions of the Vlasov Equation with Particle Simulations of Collisionless Plasmas

JACQUES DENAVIT

Plasma Physics Branch
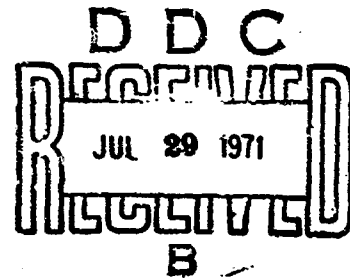*Plasma Physics Division*

AND

W. L. KRUER

Plasma Physics Laboratory
Princeton, New Jersev

June 1971

D D C
JUL 29 1971
B

NAVAL RESEARCH LABORATORY
Washington, D.C.

DOCUMENT CONTROL DATA - R & D

(Security classification of title, body of abstract and indexing annotation must be entered when the overall report is classified)

1 ORIGINATING ACTIVITY (Corporate author)	2a. REPORT SECURITY CLASSIFICATION
Naval Research Laboratory Washington, D.C. 20390	UNCLASSIFIED
	2b. GROUP ---

3 REPORT TITLE

COMPARISON OF NUMERICAL SOLUTIONS OF THE VLASOV EQUATION WITH PARTICLE SIMULATIONS OF COLLISIONLESS PLASMAS

4. DESCRIPTIVE NOTES *(Type of report and inclusive dates)*

This is an interim report on a continuing problem.

5. AUTHOR(S) *(First name, middle initial, last name)*

Jacques Denavit, and W. L. Kruer

6. REPORT DATE	7a. TOTAL NO. OF PAGES	7b. NO OF REFS
June 1971	42	27

8a. CONTRACT OR GRANT NO. NRL Problem No. 77H02-27	9a. ORIGINATOR'S REPORT NUMBER(S)
b. PROJECT NO. DASA Subtask No. HC 04001	NRL Memorandum Report 2276
c. DASA HC-04001	9b. OTHER REPORT NO(S) (Any other numbers that may be assigned this report)
d.	

10. DISTRIBUTION STATEMENT

Approved for public release; distribution unlimited.

11 SUPPLEMENTARY NOTES	12. SPONSORING MILITARY ACTIVITY The work reported herein was funded by the Defense Atomic Support Agency and the Atomic Energy Commission. Defense Atomic Support Agency, Washington, D.C. 20305

13. ABSTRACT

This paper presents numerical solutions of the Vlasov and Poisson equations for several physically significant problems and compares these solutions with the results of particle simulations. The numerical solutions of the Vlasov equation are based on the Fourier-Fourier transform method. The spatial representation includes up to 85 modes and is capable of representing strong nonlinear effects. The particle simulations are based on a multipole expansion of finite-size particles about their nearest grid point location. Special techniques are used to suppress the noise and to accurately control the initial conditions of the plasmas so that quantitative comparisons with Vlasov solutions can be made. Close quantitative agreement between the results of the two simulation techniques is observed. The problems considered are one-dimensional, with periodic boundary conditions, and involve (1) two-stream instabilities, with equal and unequal electron beams, and (2) large-amplitude electron oscillations, with sideband instabilities.

DD FORM 1473 (PAGE 1)
1 NOV 65

S/N 0101-807-6801

14 KEY WORDS	LINK A		LINK B		LINK C	
	ROLE	WT	ROLE	WT	ROLE	WT
Collisionless plasmas						
Numerical solutions						
Vlasov and Poisson equations						
Fourier-Fourier method						
Fourier-Hermite method						

DD , FORM , NOV 65 **1473** (BACK)

(PAGE 2)

40

Comparison of Numerical Solutions of the Vlasov Equation
with Particle Simulations of Collisionless Plasmas

J. Denavit
Plasma Physics Division, Naval Research Laboratory
Washington, D. C. 20390

and

W. L. Kruer
Plasma Physics Laboratory, Princeton University
Princeton, New Jersey 08540

ABSTRACT

This paper presents numerical solutions of the Vlasov
and Poisson equations for several physically significant
problems and compares these solutions with the results of
particle simulations. The numerical solutions of the Vlasov
equation are based on the Fourier-Fourier transform method.
The spatial representation includes up to 85 modes and is
capable of representing strong nonlinear effects. The particle
simulations are based on a multipole expansion of finite-size
particles about their nearest grid point location. Special
techniques are used to suppress the noise and to accurately
control the initial conditions of the plasmas so that quantita-
tive comparisons with Vlasov solutions can be made. Close
quantitative agreement between the results of the two simula-
tion techniques is observed. The problems considered are

one-dimensional, with periodic boundary conditions, and involve

(1) two-stream instabilities, with equal and unequal electron

beams, and (2) large-amplitude electron oscillations, with side-

band instabilities.

PROBLEM STATUS

This is an interim report on a continuing problem.

AUTHORIZATION

NRL Problem H02-27
DASA HC-040

ii

I. INTRODUCTION

Numerical simulation of collisionless plasmas may be achieved by either numerically solving the Vlasov and Poisson equations, or by computing the motions of a large number of charged particles that are moving in their self-consistent electric field. Although the two methods seek the same ends, they differ fundamentally in their approach and comparison of their results is not trivial.

This paper presents numerical solutions of the Vlasov and Poisson equations for several physically significant problems, and compares those solutions with the results of particle simulations. Close quantitative agreement is found. Such comparisons provide insight into the validity and limitations of both methods. The problems considered are one-dimensional with periodic boundary conditions, and involve only electrons moving over a uniform positively charged background.

Numerical solutions of the Vlasov and Poisson equations have been carried out by following the distribution function directly in phase plane,[1-3] and by transform methods. The most significant transform methods to date are, the Fourier-Fourier method,[4] in which the distribution function is Fourier-transformed with respect to both position and velocity, and the Fourier-Hermite method,[5] in which the distribution function is Fourier-transformed with respect to position and its velocity dependence is represented by a series using Hermite polynomials. The numerical solutions presented here are based on the Fourier-Fourier method. Earlier solutions based on this

1

method had been limited to two or three modes in the spatial representation. The present solutions include up to 85 modes and are capable of representing strong nonlinear effects.

Particle simulation of plasmas has been applied to a variety of problems.[6-8] In this method, quantities such as the electric field, or mean velocity, which depend on moments of the distribution function, are subject to random noise. Special techniques are used in the present solutions to suppress this noise and to accurately control the initial conditions of the plasma so that quantitative comparisons with Vlasov solutions can be made.

Section II of the paper reviews the Fourier-Fourier method used in the solution of the Vlasov equation, which in its main features follows the method of Knorr.[4] A similar review of the particle simulation method and initialization techniques is given in Sec. III. This is followed in Sec. IV by the results of comparative studies of the two methods for four cases. These cases were chosen among problems which had been considered earlier in the literature, so that comparison could be made not only between the present solutions, but also with earlier numerical studies.

For both the Vlasov and particle solutions presented here, time is measured in units of ω_p^{-1}, where ω_p is the plasma frequency, length is measured in units of the periodicity length L of the system, and velocity is measured in units of $L\omega_p$. It follows that the electric field is measured in units of $mL\omega_p^2/e$, where e and m are the electron charge and mass, respectively.

II. FOURIER-FOURIER TRANSFORM METHOD

In terms of the above units, the one-dimensional Vlasov equation for electrons takes the form:

$$\frac{\partial f}{\partial t} + v \frac{\partial f}{\partial x} - E \frac{\partial f}{\partial v} = 0 \qquad , \qquad (1)$$

where $f(x, v, t)$ denotes the one-dimensional electron distribution function and $E(x, t)$ is the electric field. Let $E(x, t) = E^{ext}(x, t) + E^{int}(x, t)$, where E^{ext} is an external field and E^{int} is the internal field due to electrons and the positively charged background. The internal field is determined by Poisson's equation

$$\frac{\partial E^{int}}{\partial x} = 1 - \int_{-\infty}^{+\infty} f \, dv \qquad . \qquad (2)$$

Taking Fourier transforms of the distribution function with respect to position and velocity and applying periodic boundary conditions in space with periodicity length $L = 1$ yields

$$H_n(q, t) = \int_{-\infty}^{+\infty} \exp(iqv) \, dv \int_0^1 f(x, v, t) \exp(-2\pi i n x) \, dx \qquad .$$

The functions $H_n(q, t)$ are the characteristic functions[9] for each mode. n denotes the mode number in space, and q is the velocity transform variable. A Fourier transform in space of $E(x, t)$ yields the modes of the electric field,

$$\overline{E}_n(t) = \int_0^1 E(x, t) \exp(-2\pi i n x) \, dx \qquad .$$

Since $f(x, v, t)$ and $E(x, t)$ must be real valued, we have

3

$$H_{-n}(q, t) = H_n^*(-q, t) \quad ,$$

(3)

$$\bar{E}_{-n}(t) = \bar{E}_n^*(t) \quad .$$

After transformation and truncation at a finite number of modes m_{max}, which will be retained in numerical computations, the Vlasov equation yields

$$\frac{\partial H_n}{\partial t} + 2\pi n \frac{\partial H_n}{\partial q} = \frac{q}{2\pi} C_n(q, t) \quad ,$$

(4)

where

$$C_n(\,,t) = -2\pi i \sum_{m=-m_{max}}^{m_{max}} \bar{E}_m(t) H_{n-m}(q, t)$$

(5)

is a convolution term which comes from the nonlinear term of the Vlasov equation. Poisson's equation gives

$$-2\pi i \, \bar{E}_n^{int} = \frac{1}{n} H_n(q = 0) \qquad \text{for } n \neq 0$$

and $\bar{E}_o^{int} = 0$.

Equations (4) are solved by integration along their characteristics, which are straight lines of slope $2\pi n$ in the (t, q) plane, as shown in Fig. 1. At each time step, the value of $H_n(q, t)$ is obtained from the iterative formula

$$H_n^{(i+1)}(q, t) = H_n(q - 2\pi n \Delta t, t - \Delta t) + \frac{1}{4\pi}(q - 2\pi n \Delta t) \Delta t \, C_n(q - 2\pi n \Delta t, t - \Delta t)$$

$$+ \frac{1}{4\pi} q \Delta t \, C_n^{(i)}(q, t) \quad ,$$

(6)

in which the superscript denotes the number of iterations carried out. The results presented in this paper were obtained using a single iteration.

4

From the definition of the convolutions C_n, Eq. (6) gives the improved approximations $H_n^{(i+1)}$, for $n = m_{max}, \ldots, + m_{max}$, in terms of linear combinations of the preceding approximations $H_n^{(i)}$. The matrix of the coefficients of these linear combinations is

$$
\Lambda = -\frac{iq\Delta t}{2}
\begin{bmatrix}
0 & \overline{E}_{-1} & \overline{E}_1 & \overline{E}_{-2} & \cdots \\
\overline{E}_1 & 0 & \overline{E}_2 & \overline{E}_{-1} & \cdots \\
\overline{E}_{-1} & \overline{E}_{-2} & 0 & \overline{E}_{-3} & \cdots \\
& & \cdots\cdots &
\end{bmatrix}
$$

and the iterative process defined by Eq. (6) converges only if all eigenvalues λ_j, for $j = -m_{max}, \ldots, + m_{max}$, of this matrix are smaller than unity. Letting Λ^T denote the transposed matrix of Λ, we have

$$
|\lambda_j|^2 \leq \text{Trace}\,(\Lambda\,\Lambda^T) = (q\Delta t)^2\, m_{max}\, U \quad,
$$

where U is the total electrostatic energy. The iterative process is convergent, therefore, if

$$
q_{max}\, \Delta t\, (m_{max}\, U)^{1/2} < 1 \quad, \tag{7}
$$

where q_{max} is the maximum value of q retained in the computation. This criterion is satisfied by adjusting the time step Δt according to the magnitude of the electrostatic energy.

Values of q in Eq. (6) are chosen to fall at grid points, as shown in Fig. 1. The values of H_n at $q - 2\pi n \Delta t$, then, do not fall at the grid points, and must be interpolated using neighboring points. A nine-point Lagrangian

interpolation was used in the computations presented. If Δq denotes the interval between grid points, we expect the distribution function $f(x, v, t)$ to be adequately defined over the interval $-v_{max} < v < v_{max}$ in which $v_{max} \simeq 1/\Delta q$.

The characteristic functions $H_n(q, t)$, for $n = 0, \ldots, m_{max}$ are evaluated over the interval $-q_{max} \leq q \leq q_{max}$. Values of $H_n(q, t)$ for negative values of n are found from the reality conditions (3). At the lower boundary, $q = -q_{max}$, the values of $H_n(q - 2\pi n \Delta t, t - \Delta t)$ needed in Eq. (6) are unknown. These values are set equal to zero, thus introducing a cutoff for the characteristic functions at $q = \pm q_{max}$. The introduction of cutoffs m_{max} and q_{max} is equivalent to a smoothing of the distribution function $f(x, v, t)$ defined by

$$\tilde{f}(x, v, t) = \int_{-\infty}^{+\infty} w_v(v') \, dv' \int_0^1 w_x(x') \, f(x + x', \, v + v', t) \, dx'$$

where $\tilde{f}(x, v, t)$ is the smoothed distribution function, and

$$w_x(x) = 1 + 2 \sum_{n=1}^{m_{max}} \cos 2\pi n x$$

and

$$w_v(v) = \frac{\sin q_{max} v}{\pi v}$$

are weight functions. The function w_x has a half-width $\Delta x \simeq 1/2 m_{max}$, and the function w_v has a half width $\Delta v \simeq \pi/q_{max}$. The choice of the cutoff values m_{max} and q_{max} must be made so that the half-widths Δx and Δv are small compared to characteristic lengths and velocities in the plasma.

6

The particle code considered in this paper uses finite-size particles having a Gaussian charge distribution with half-width a (see Sec. II'). After Fourier transformation in space and application of Poisson's equation, this is equivalent to multiplying the electric field $\overline{E}_m$ of each mode by the form factor $W_m = \exp[-(2\pi a m)^2]$. To represent the effect of finite-size particles in the Vlasov solution, this form factor may be incorporated into the convolution term:

$$C_n(q,t) = -2\pi i \sum_{m=-m_{max}}^{m_{max}} W_m \overline{E}_m(t) H_{n-m}(q,t) \quad . \tag{8}$$

This modified form of the convolution reduces to the original form given by Eq. (5) if the form factor W_m is set equal to unity.

The introduction of the form factor W_m modifies the dispersion relation of the plasma, which becomes

$$2\pi n + W_n \int_{-\infty}^{+\infty} \frac{\partial f_o/\partial v}{\omega - 2\pi n v} \, dv = 0 \quad ,$$

where n is the mode number and ω the corresponding complex frequency.

The kinetic energy is given by

$$T = -\frac{1}{2} \left(\frac{\partial^2 H_o^R}{\partial q^2} \right)_{q=0} \quad , \tag{9}$$

where $H_o^R(q,t)$ is the real part of $H_o(q,t)$ and the electrostatic energy is given by

$$U = \sum_{n=1}^{m_{max}} \frac{W_n}{(2\pi n)^2} \left| H_n(q = 0, t) \right|^2 \quad . \tag{10}$$

7

Each term of the convolution array C_n is the sum of m_{max} terms. Since there are m_{max} terms in the array, the computing time required to evaluate the convolution by direct summation is proportional to m_{max}^2. The computing time is significantly reduced by using discrete Fourier transforms to evaluate the convolution. The arrays $H_n(q,t)$ and $\bar{E}_n(t)$ are Fourier-transformed, their transforms are multiplied, and an inverse transform of the product is carried out to obtain the convolution array C_n. Since H_n and $\bar{E}_n$ are not defined cyclically, but instead are zero for $|n| > m_{max}$, it is necessary to append zeros to both ends of the arrays before carrying out the transforms. Using a fast Fourier transform algorithm,[10,11] the computing time becomes proportional to $m_{max} \log_2 m_{max}$. This method is advantageous for $m_{max} > 10$.

III. PARTICLE SIMULATION METHOD

The particle code investigates the electrostatic behavior of a plasma by simply following the motion of a large number of electrons in their self-consistent (and any externally imposed) fields. Such codes are widely used in computational plasma physics.[6-8] The basic scheme consists of a very simple cycle. The positions of the particles determine the charge density, which by Poisson's equation gives the self-consistent electric field. In one dimension and in terms of the dimensionless units used in this paper, Poisson's equation takes the form

$$\frac{\partial E^{int}}{\partial x} = \frac{1}{N} \sum_{j=1}^{N} \rho_j(x) \quad ,$$

8

where $\rho_j(x)$ is the charge density contributed by particle j and N is the total number of particles. The particle velocities and positions are then updated by the laws of dynamics, using a standard leapfrog scheme

$$\dot{v} = -E$$

$$\dot{x} = v \quad .$$

Continuing about this basic cycle advances the system in time. Of course, one must use a time step sufficiently small to accurately follow the time variation of the forces in the system. One tenth of ω_p is generally adequate.

In these codes one also inevitably needs to discretize space, i.e., to introduce a regularly spaced grid. How one then defines the relevant physical quantities on that grid is the principal place where various particle codes differ. We here use a multipole expansion scheme[12,13] and finite-size particles. The charge density is then defined on the grid by a multipole expansion of the particle's charge density about its nearest grid-point location. We briefly illustrate the procedure: Consider a particle j with a Gaussian charge distribution having a half-width a.

$$\rho_j(x) = -\frac{\exp\left[-(x-x_j)^2/2a^2\right]}{(2\pi)^{1/2}\, a} \quad .$$

Here x_j is the center-of-mass location of the particle. Introduce a grid and describe the particle position as $x_j = n\delta + \Delta x_j$, where δ is the cell size and n denotes the nearest grid-point location. Δx_j is at most $\delta/2$. Hence, assuming $\delta/2a \ll 1$, we expand the charge density as follows:

9

$$\rho_j(x) = - \frac{\exp[-(x-n\delta)^2/2a^2]}{(2\pi)^{1/2} a} \left[1 + \frac{(x - n\delta)}{a^2} \Delta x_j + \dots \right] \qquad .$$

Clearly we are replacing the finite-size particle centered somewhere in the cell, by a finite-size particle centered at the nearest grid point, plus a finite-size dipole there, plus (in principle) higher-order multipole terms. In practice we stop at the dipole correction. Summing over a collection of particles and introducing a Fourier transform gives the total charge density in Fourier transform space as

$$\rho(k) = - \exp(-k^2 a^2/2) \sum_n \exp(-ikn\delta) \left[Q(n) - ikP(n) + \dots \right] \qquad .$$

Here $Q(n)$ and $P(n)$ are arrays giving the net monopole and dipole moments associated with the $\underline{n}$th grid point. Notice the form factor $\exp(-k^2 a^2/2)$, which arises due to the finite particle size. The electric field is now determined simply by an inverse Fourier transform. The force on the particle is given by the same multipole expansion procedure. Physically this amounts to representing the force on the finite-size particle as its monopole moment times the electric field, plus the dipole moment times the derivative of the field.

The multipole expansion scheme is very appealing. First, it represents a systematic and physical way to introduce the spatial grid. Indeed, an expansion parameter has been exhibited. Charge-sharing schemes[7,8] can be related to the multipole expansion by stopping at the dipole approximation and representing derivative terms by a difference over cells. Second, the multipole expansion scheme relates the numerical approximation resulting from

introducing a grid to physical concepts. One is investigating the physics of a plasma of finite-size particles, and hence there are some modifications of the plasma behavior.[14] In general, the finite size of the particle enters the analysis via the form factor, the Fourier transform of the particle charge distribution. For example, for Gaussian particles, the form factor is $\exp(-k^2 a^2/2)$. We see that the long-wavelength (collective) behavior of the system is essentially unaltered, but the short-wavelength ($ka > 1$) behavior is systematically suppressed. This is welcome, since short-wavelength behavior ($\lambda <$ cell size) cannot be represented accurately due to the finite size of the grid. Furthermore, its suppression lowers the noise level and hence lowers the effective collision frequency.[15] This yields more realistic simulations with fewer particles.

A further technique used for reducing the noise level in the particle code is known as a "quiet start."[16] A quiet start simply refers to beginning the calculation with ordered initial conditions. Basically, no random numbers are used to set up the calculations. A set of J discrete velocities is chosen using the probability function

$$p = P(v) = \int_{-\infty}^{v} f(v)\, dv \quad ,$$

where $f(v)$ is the desired velocity distribution function. The procedure is illustrated in Fig. 2 for the case of a Maxwellian distribution function. A set of J values, $p_j = (j - 0.5)/J$ with $j = 1, \ldots, J$, are chosen, equally spaced between $p = 0$ and $p = 1$. The corresponding velocities, $v_j = P^{-1}(p_j)$, are then

11

distributed according to the distribution function f(v).[17] Sets with J varying from 100 to 1600 were used in the present computations. Equal numbers of particles are then loaded at each grid point. The particles may be loaded identically at all grid points using all the velocities in the set $\{v_j\}$, and J particles per cell are then needed. However, the particles form a number of discrete small beams, which are subject to instabilities, and spurious oscillations may appear.[18] This difficulty is reduced by using a larger number of beams. To achieve this without increasing the total number of particles, the particle velocities are staggered so that each discrete velocity is repre-sented only at every kth grid point. For example, the set of velocities may be divided into k subsets by picking every kth value of the original set. The particles are then loaded at different grid points with different subsets, repeat-ing the same loading every kth cell. The repetition length kδ should be much smaller than any physical length of interest in the problem.

The quiet start eliminates the initial noise level, and indeed leaves one the option of starting the computations with specified initial conditions. An initial density distribution $\rho(x)$ may be obtained by giving the particles initial displacements from their uniform distribution at the grid points. If $\xi(x)$ denotes the displacement of a particle loaded at x, and ρ_o denotes the uniform density before displacements, then $\xi(x)$ is found by integrating the equation

$$\frac{d\xi}{dx} = \frac{\rho_o}{\rho(x + \xi)} - 1 \quad .$$

The possibility of controlling initial conditions is important for detailed comparisons with other codes—in particular, with the Vlasov code considered in this paper.

IV. RESULTS

Case A

Consider a two-stream instability resulting from the initial conditions
defined by the distribution function

$$f(x, v, t = 0) = f_o(v) [1 + 2\epsilon \cos 2\pi x] \quad , \tag{11}$$

with

$$f_o(v) = \frac{1}{(2\pi)^{1/2} v_{th}^3} v^2 \exp(-v^2/2v_{th}^2) \tag{12}$$

and $v_{th} = 0.30/\pi$, $\epsilon = 2.5 \times 10^{-2}$. These initial conditions correspond to a
system length $L = 10.5 \lambda_D$. The initially excited mode, as shown in Eq. (11),
has a wavelength equal to the length of the system. The linear growth rates
for this problem have been computed by Grant and Feix.[19] The first mode
is the only unstable mode and has a growth rate $\gamma = 0.25$. Vlasov solutions
for this problem have been carried out by Armstrong and Montgomery[20]
using the Fourier-Hermite method. Comparisons between Fourier-Hermite
solutions and particle-in-cell solutions have also been made by Armstrong
and Nielson.[21]

The solid curve in Fig. 3 corresponds to the total electrostatic energy for
the Vlasov solution, with $m_{max} = 21$, $q_{max} = 256$, and $\Delta q = 4$. This energy
grows at approximately the linear growth rate from t = 10 to t = 20, and
saturates at 2.2% of the total energy. At the time of saturation, the bounce
frequency of electrons in the unstable large wave (0.33) is roughly equal to

13

the linear growth rate of the instability (0.24). This is a reasonable result for saturation, since a large wave significantly modifies the particle dynamics in a time ~ $1/\omega_B$. After saturation, the electrostatic energy oscillates with a period of approximately 20. The frequency of trapped electron oscillations at saturation is $\omega_B = 0.33$, which corresponds to a trapping period $\tau_{TR} = 19.2$.

The amplitude of the first mode ($n = 1$) is approximately an order of magnitude larger than the amplitudes of the other modes ($n \geq 2$). The higher modes, however, have a significant effect on the solution, as shown by the broken line in Fig. 3 (which corresponds to $m_{max} = 10$). The Vlasov solution was checked by reversing it at $t = 20$, and the small broken line near $t = 0$ in Fig. 3 shows the deviation.

The circles in Fig. 3 correspond to the particle solution with 51,200 particles and 256 cells. The particle half-width is $a = 1.25\delta$, where δ is the cell size. The initial particle positions and velocities were chosen to match the initial conditions of the Vlasov solution, using the quiet-start method of Sec. III with 1600 velocities. Since there were 200 particles per cell, the initial velocity distribution was repeated every 8 cells.

Conservation of energy was checked in both the Vlasov and particle solutions. The relative energy error is 2×10^{-4} for the Vlasov solution and 1.2×10^{-4} for the particle solution. To give some idea of the computing time, the unoptimized Vlasov code required ~ 13 min. on the 360/91 for this problem. This compared reasonably with the time of ~ 15 min. required by the unoptimized particle code.[22]

14

Several additional runs on the particle code were made to investigate spurious oscillations which had been observed in earlier runs with fewer discrete beams. The solid line in Fig. 4 shows the electrostatic energy when 100 particles are loaded identically at every grid point, thus forming 100 discrete beams. In contrast to the smooth behavior of the 1600-beam case shown in Fig. 3, strong oscillations of the fundamental ($n = 1$) with a frequency $\omega \simeq 2$ are now superimposed. These oscillations may be attributed to beaming instabilities, since they do not appear when the number of beams is increased. With the present quiet-start technique, the most unstable beams are those representing the tails of the distribution function, since they are the most widely separated. With 100 discrete velocities, the last three beams are located at $v_b = 2.78$, 2.99, and 3.37 v_{th}, respectively. The frequency of beaming instabilities is given by $\omega \simeq kv_b$, where k is the wave number. In the present case, k corresponds to the fundamental; i.e., $k = 2\pi$. With $v_b \simeq 3 v_{th}$, we then have $\omega \simeq 1.8$, which agrees with the observed frequency. The observed growth rate of these spurious oscillations is $\sim k\Delta V$, where ΔV is typical of the last few widely spaced beams. To confirm that the spurious oscillations are caused by the instability of beams around $v_b = 3 v_{th}$, a run was made in which only the last two beams at each end of the distribution function were staggered. The resulting electrostatic energy is shown by the broken line in Fig. 4. Indeed, the spurious oscillations now appear significantly later in time. This is expected, of course, since the less separated beams, which were not staggered, are also subject to instabilities but with smaller growth rates.

15

Case B

We now consider a second case of a two-stream instability with equal beams, in which several unstable modes are allowed to grow. The initial conditions for this case are

$$f(x, v, t = 0) = f_o(v) \quad [1 + 2\epsilon \sum_{n=1}^{21} \cos(2\pi n x + \phi_n)] \quad , \tag{13}$$

with

$$f_o(v) = \frac{1}{2(\pi)^{1/2} v_p} [\exp -(v+v_d)^2/v_p^2 + \exp -(v-v_d)^2/v_p^2] \quad , \tag{14}$$

and $v_p = \sqrt{2} \times 10^{-2}$, $v_d = 2v_p$, $\epsilon = 5 \times 10^{-3}$. The initial phase angles ϕ_n are chosen at random in the interval $(0, 2\pi)$. These initial conditions correspond to a system length of $100 \lambda_D$, and the dispersion relation shows that modes 1 to 6 are unstable. This case was studied by Morse and Nielson[23] using the particle-in-cell method.

The total electrostatic energy for the Vlasov solution is given by the solid line in Fig. 5. This solution was carried out with $m_{max} = 21$, $q_{max} = 1000$ and $\Delta q = 15.6$. The electrostatic energy reaches approcimately 6.7% of the total energy. We again observe that the instability saturates when the electron bounce frequency in the dominant wave (0.28) is approximately equal to its linear growth rate (0.26).

The broken line in Fig. 5 corresponds to the particle solution with 25,600 particles and 256 cells. A quiet start was used to match the initial conditions of the Vlasov code, including the same values of the phase angles ϕ_n. Only

100 velocities were used. The discrete beams set up by the quiet-start method are rapidly disrupted by the collective instability in the present case, and no spurious instabilities are observed. The relative energy error is 1.2×10^{-4} for the Vlasov solution, and 0.8×10^{-3} for the particle solution.

Comparisons of densities in phase space for the Vlasov and particle solutions at different times are given in Figs. 6, 7, and 8. For the Vlasov solutions, numbers from 1 to 9 denote relative densities. Blanks correspond to densities which are less than one tenth of the maximum density. Negative signs correspond to negative values of the density, which occur because no form factors were used in the present computation. For the particle solution, an asterisk was printed at every location where at least one particle is present.

The results of Morse and Nielson for this case agree qualitatively with the present results. The electrostatic energy in their case reaches only 5% of the total energy, and does not give the two distinct peaks shown in Fig. 5. However, the case considered by Morse and Nielson corresponded to a longer system length ($L = 500\, \lambda_D$). In addition, these authors did not control the initial conditions of their computations, but allowed the instability to grow from the noise resulting from a random choice of initial particle velocities. Their phase density plots agree with those of Figs. 6, 7, and 8, showing the same coalescing of the eddies when their system's length of $500\, \lambda_D$ is taken into account.

17

Case C

We now examine an instability resulting from the interaction of a small beam with a Maxwellian plasma. The initial conditions are

$$f(x, v, t = 0) = f_o(v) \left[1 + 2\epsilon \sum_{n=1}^{21} n \cos(2\pi n x + \phi_n) \right] \quad , \tag{15}$$

with

$$f_o(v) = \frac{1}{\sqrt{\pi} \, v_p} \left\{ n_p \exp(-v^2/v_p^2) + n_b \exp[-(v-v_d)^2/v_b^2] \right\} \quad . \tag{16}$$

Here $v_p = (1/\sqrt{2}) \, 10^{-2}$, $v_d = 2.6 \, v_p$, $v_b = 0.25 \, v_p$, $n_p = 0.95$, $n_b = 0.05$, $\epsilon = 2.5 \, 10^{-4}$ and the initial phase angles ϕ_n are chosen at random. Thus the small beam contains 5% of the plasma, and its mean velocity is 3.66 thermal velocities. These initial conditions correspond to a system length of $100 \, \lambda_D$. The dispersion relation shows that modes 1 to 9 are now unstable. This case was also studied by Morse and Nielson,[23] using the particle-in-cell method.

The total electrostatic energy for the Vlasov solution without form factors is shown by the solid line in Fig. 9. This solution was carried out with $m_{max} = 42$, $q_{max} = 25/v_p$, and $\Delta q = q_{max}/128$. The electrostatic energy reaches 1.6% of the total energy. Again the instability saturates when the electron bounce frequency in the dominant mode (0.16) is approximately equal to its linear growth rate (0.15).

It has generally been found that each trapping region requires a minimum of 8 to 10 modes for its representation. In Case A, where the most unstable

18

mode is the fundamental one and a single trapping region is present through the system, qualitatively correct results were obtained with $m_{max} = 10$. In the present case, mode $m = 5$ is the most unstable, and 42 modes were found to be necessary to obtain a convergent solution. A solution with $m_{max} = 10$ gave qualitatively different results beyond saturation. For $\omega_p t > 40$, the $m_{max} = 10$ solution gave trapping oscillations which continued to grow in amplitude instead of dropping to the low levels shown in Fig. 9.

The circles in Fig. 9 correspond to the particle solution with 61, 440 particles and 256 cells. A quiet start was used again, to match the initial conditions of the Vlasov solutions. In the present case, 960 velocity classes were used to maintain the small-beam instabilities at a low level. The relative energy error was $\simeq 10^{-4}$ for the Vlasov solution and $\simeq 3 \ 10^{-4}$ for the particle solution.

The results of Morse and Nielson in this case again agree qualitatively with the present results. The saturation electrostatic energy in their solution was 2% of the total energy instead of the 1.6% in the present solutions. This difference may again be due to the longer length of their system (200 λ_D) and to random initial perturbations.

Case D

This case is concerned with sideband instabilities resulting from the motion of trapped particles in a large-amplitude electrostatic wave. The excitation of large-amplitude waves by means of an electrostatic probe immersed in a warm plasma has been described by Wharton, Malmberg,

19

and O'Neil.[24] These experiments showed the expected amplitude modulation of the wave, which is attributed to electron trapping, but they also disclosed the appearance of sidebands to the frequency of the main wave. The growth of these sidebands has been attributed by Kruer, Dawson, and Sudan[25] to an instability due to particles trapped in the large-amplitude wave, and has been observed by Kruer and Dawson in particle simulations.[26]

In the present computations, the initial distribution function of the plasma is defined by

$$f(x, v, t = 0) = f_o(v) \left[1 + 2\epsilon \sum_{n=1}^{42} n \cos(2\pi n x + \phi_n) \right] \quad , \tag{17}$$

with

$$f_o(v) = \frac{1}{(2\pi)^{1/2}} \exp\left[-(v^2/2v_{th}^2) \right] \quad . \tag{18}$$

Here $v_{th} = 1.06/44\pi$, $\epsilon = 0.0002$ and the initial phase angles are chosen at random. These initial conditions correspond to a plasma length $L = 130 \lambda_D$. Mode $n = 5$ is then driven from $t = 0$ to $t = 6$ by the external field[27]

$$E^{ext}(x, t) = E_{DR} \sin(\omega_o t + kx) \quad , \tag{19}$$

with $E_{DR}/v_{th} = 0.3$ and $\omega_o = 1.06$. The driving frequency ω_o is the Bohm-Gross frequency corresponding to mode $n = 5$. and the ratio of the phase velocity of the driving wave to the thermal velocity is $\omega_o/2\pi n v_{th} = 4.4$.

The electrostatic energies of the main wave and sidebands from the Vlasov and particle solutions are compared in Figs. 10 and 11. The particle solution was carried out with 256 cells and 200 particles per cell. A quiet start

20

was used with 1600 discrete velocities to represent the distribution function. The particles were given displacements to match the initial density perturbation defined by Eq. (17). The particle half-width was $a = 2\delta = \lambda_D$, where δ is the cell length. The Vlasov solution was carried out with $m_{max} = 42$, thus allowing approximately 8 modes for each trapping region. The truncation in velocity transform was at $q_{max} = 8/v_{th}$ and the grid spacing was $\Delta q = 1/8 v_{th}$. These values correspond to a velocity resolution $\Delta v \simeq \pi/q_{max} \simeq v_{th}/4$ and a maximum velocity $v_{max} \simeq 1/\Delta q = 8 v_{th}$. A form factor was applied to the electric field of the Vlasov solution corresponding to the particle half-width $a = \lambda_D$ used in the particle code. The relative energy error was 4×10^{-4} for the particle solution and 3×10^{-4} for the Vlasov solution.

The main wave energy (electrostatic energy of mode $n = 5$) and the lower sideband energy (sum of the electrostatic energies of modes $n = 1$ to 4) are shown in Fig. 10 on a logarithmic scale. The main wave energy rises rapidly during the driving period to 29.4% of the initial kinetic energy, after which it oscillates with approximately the trapping oscillation period ($\tau_{TR} = 20.7$). We observe close agreement between the Vlasov and particle solutions for the main wave. Indeed, the two curves are nearly identical until late in the simulation. The lower sideband energy from the Vlasov and particle solutions grows at the same rate (a ten-folding time of ~ 31) and even saturates at the same level. The lower sidebands saturate when they acquire an energy comparable to that of the large wave. Then the sideband waves disrupt the particle trapping in the original large wave, as confirmed by phase space plots. It should be emphasized that this problem is very nonlinear and is a

21

strong test of both of the simulation techniques. We are accurately following not only sizeable oscillations in the large wave energy, but also simultaneous growth of oscillations at other wave numbers.

The upper sideband energy from both solutions is shown in Fig. 11. The main wave energy has been repeated on this figure to provide a reference. Again, the two solutions agree well and even saturate at the same level. The saturation level of the upper sideband is approximately an order of magnitude below the saturation level of the lower sidebands. This lower saturation level is reasonable since the upper sidebands have phase velocities less than that of the main wave and hence are more readily damped by the particles.

Several additional solutions were carried out with both the Vlasov and the particle codes. The Vlasov solutions included a computation with $m_{max} = 85$ and a weaker form factor ($a = \lambda_D/2$). This computation showed only minor variations from the results of Figs. 10 and 11. The particle solutions included one with fewer beams, to describe the distribution function. This calculation showed that details of the saturation levels (but not the growth rates) are sensitive to the number of beams used. This is reasonable, since the trapped particles responsible for the sidebands come from the tail of the initial distribution, which is rather poorly represented if too few beams are used.

SUMMARY

This paper has presented quantitative comparisons of particle simulations with multiple-mode solutions of the Vlasov equation including up to 85 modes. Previous solutions of this type had been limited to a few modes only. The problems considered ranged in complexity from a two-stream instability involving a single unstable mode and low electrostatic energy (2.2% of the total energy) to an instability due to particles trapped in a large-amplitude plasma wave. By using quiet starts to initialize tha particle simulations and using a sufficient number of beams to suppress beaming instabilities, close agreement was found between the two methods.

Since the two methods differ fundamentally in their approach, the agreement found confirms their validity. However, the problems considered have shown limitations in both methods, which must be taken into account in the physical interpretation of numerical simulation results. Discrete particle effects in particle simulations, which are particularly evident in regions of low density in phase space, yield beaming instabilities which must be minimized or accounted for in the physical interpretation of the results. Similarly, solutions of the Vlasov equation tend to develop increasingly fine structures with increasing time. The fine structures are suppressed by truncation of the Fourier expansions to a finite number of modes, but enough modes must be retained to make the half-widths $\Delta x = 1/2\, m_{max}$ and $\Delta v = \pi/q_{max}$ small compared to the characteristic lengths and velocities of the phenomena being considered. As indicated in the discussion of Case III, approximately 8 to 10 modes are needed to represent each trapping region and the solution may be altered in its general character if fewer modes are retained.

ACKNOWLEDGMENTS

REFERENCES

[1] G. Knorr, Z. Naturforsch. 16a, 1320 (1961).

[2] K. R. Symon, presented at the Fourth Conference on Numerical Simulation of Plasmas, Washington, D.C. (Nov. 1970, to be published); also P. H. Sakanaka, C. K. Chu, and T. C. Marshall, Phys. Fluids 14, 611 (1971).

[3] H. L. Berk and K. V. Roberts, Phys. Fluids 10, 1595 (1967).

[4] G. Knorr, Z. Naturforsch. 18a, 1304 (1967); see also T. P. Armstrong, R. C. Harding, G. Knorr, and D. Montgomery in Methods in Computational Physics, Vol. 9, B. J. Alder, S. Fernbach, and M. Rotenberg, eds. (Academic Press, New York, 1970) pp. 30-87.

[5] T. P. Armstrong, Phys. Fluids 10, 1269 (1967); see also D. Montgomery, in Statistical Physics of Charged Particle Systems, R. Kubo and T. Kihara, eds. (Syokabo, Tokyo, 1969) pp. 156-177.

[6] J. M. Dawson and R. Shanny, Phys. Fluids 11, 1506 (1968).

[7] C. K. Birdsall and D. Fuss, J. Comp. Phys. 3, 494 (1969).

[8] J. P. Boris and K. V. Roberts, J. Comp. Phys. 4, 552 (1969).

[9] H. Cramer, Mathematical Methods of Statistics (Princeton University Press, Princeton, N. J. 1946), pp. 89-103.

[10] J. W. Cooley and J. W. Tukey, Math. Comp. 19, 297 (1965).

[11] Computer programs implementing the fast-Fourier transform algorithm were contributed by J. Boris.

[12] J. M. Dawson, C. G. Hsi, and R. Shanny, Princeton Plasma Physics Laboratory MATT-719 (1969).

[13] W. L. Kruer and J. M. Dawson, Bull, Am. Phys. Soc. 14, 1025 (1969).

[14] A. B. Langdon and C. K. Birdsall, Phys. Fluids 13, 2115 (1970).

[15] H. Okuda and C. K. Birdsall, Phys. Fluids 13, 2123 (1970).

[16] J. A. Byers and M. Grewal, Phys. Fluids 13, 1819 (1970); see also R. J. Mason, Bell Telephone Labs. Whippany, N. J. Reports Nos. PCP-70-21 and 36.

[17] M. Abramowitz and I. A. Stegun eds. Handbook of Mathematical Functions (Dover, New York, 1965), pp. 952, 953.

[18] J. M. Dawson, Phys. Rev. 118, 381 (1960).

[19] F. C. Grant and M. R. Feix, Phys. Fluids 10, 696 (1967).

[20] T. P. Armstrong and D. Montgomery, J. Plasma Phys. 1, 425 (1967).

[21] T. P. Armstrong and C. W. Nielson, Phys. Fluids 13, 1880 (1970).

[22] This particle code has been optimized by B. Rosen and currently requires ~ 4 μsec/particle for the dipole approximation. The two-dimensional version of this code has been extensively optimized by the Princeton Simulation Group and currently requires ~ 5 μsec/particle for the nearest-grid-point approach.

[23] R. L. Morse and C. W. Nielson, Phys. Fluids 12, 2418 (1969).

[24] C. B. Wharton, J. H. Malmberg, and T. M. O'Neil, Phys. Fluids 11, 1761 (1968).

[25] W. L. Kruer, J. M. Dawson, and R. N. Sudan, Phys. Rev. Letters 23, 838 (1969).

[26] W. L. Kruer and J. M. Dawson, Phys. Fluids 13, 2747 (1970).
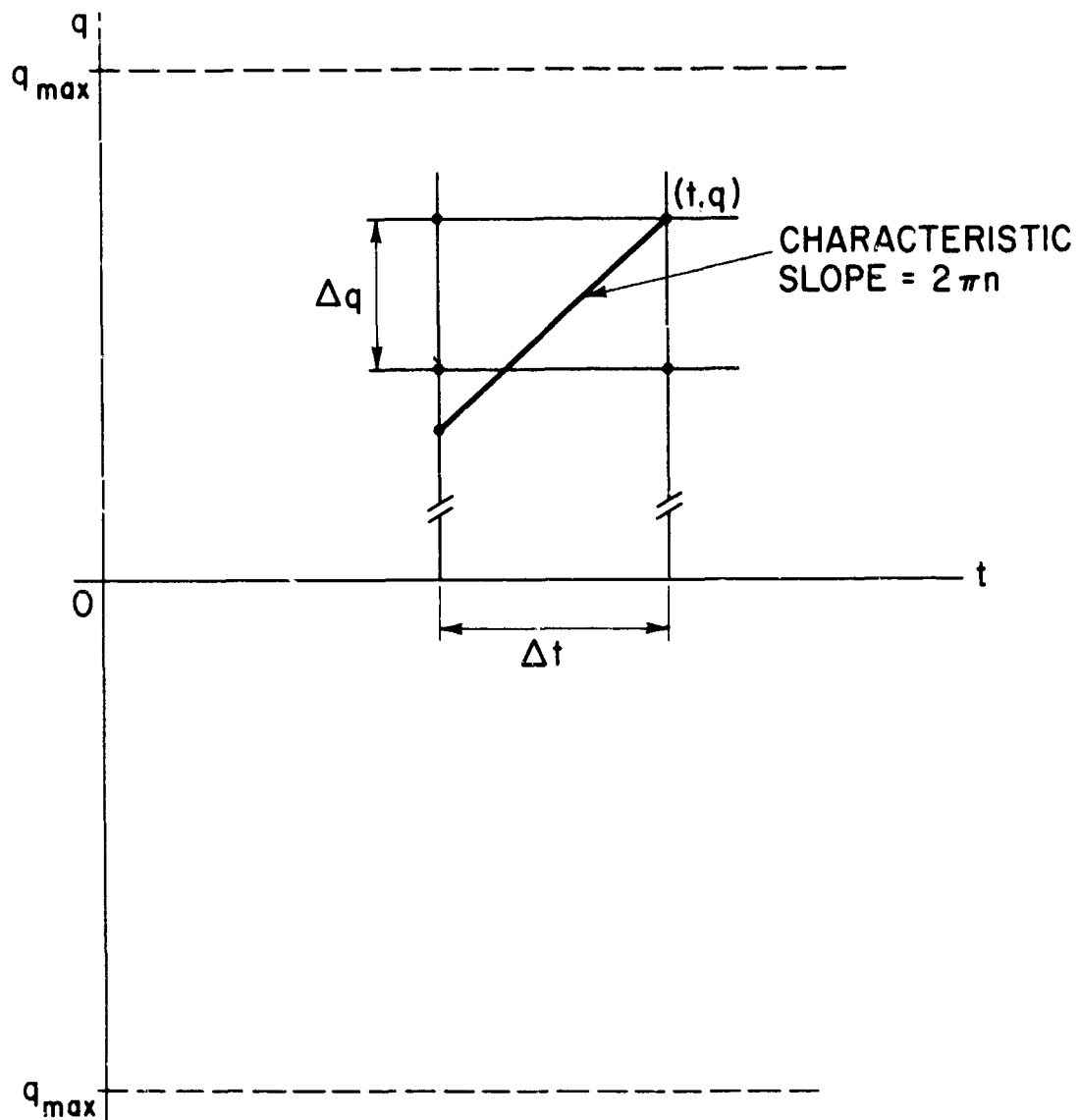
[27] R. C. Harding, Phys. Fluids 11, 2233 (1968).

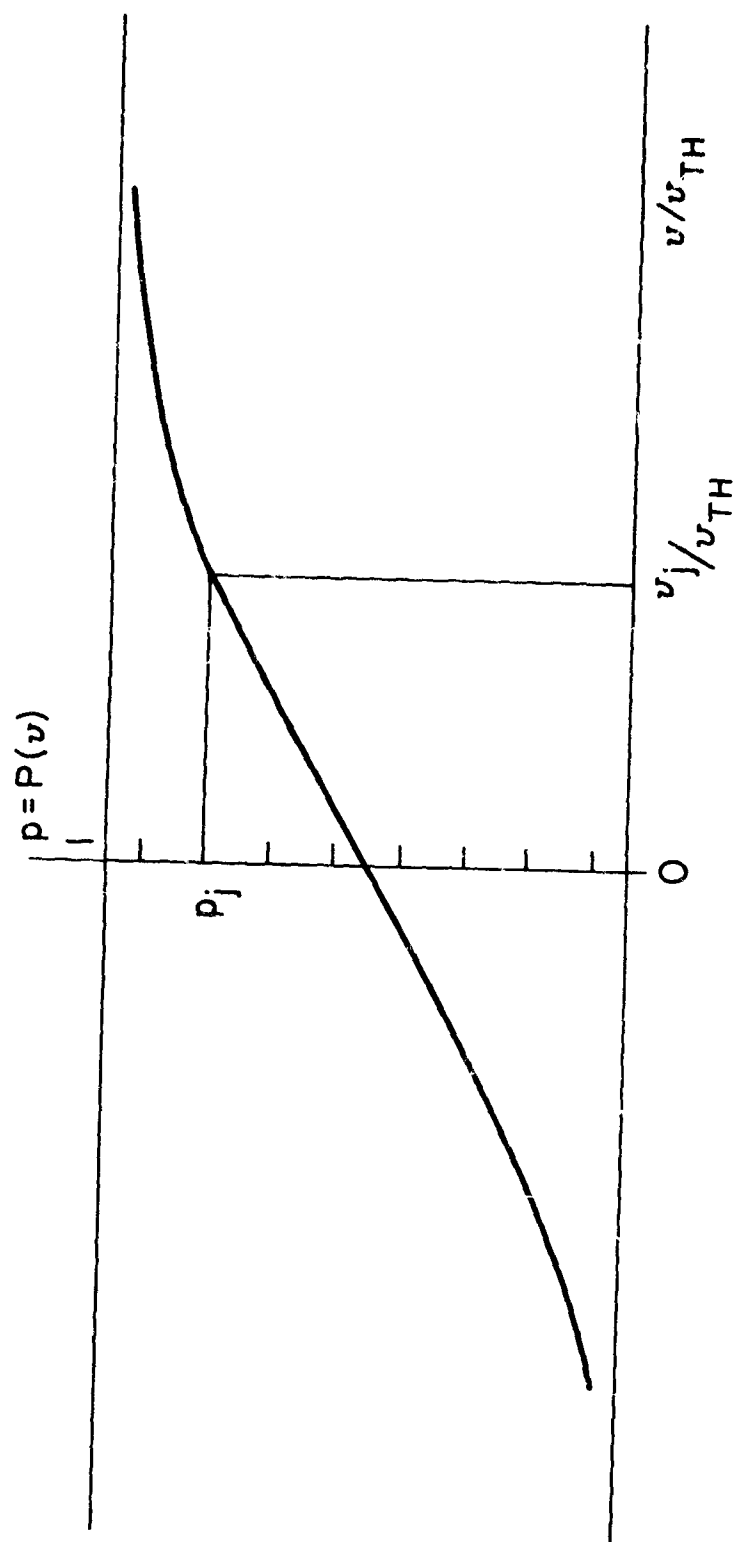Fig. 1 - Characteristics of Eq. (4) in the (t, q) plane

28

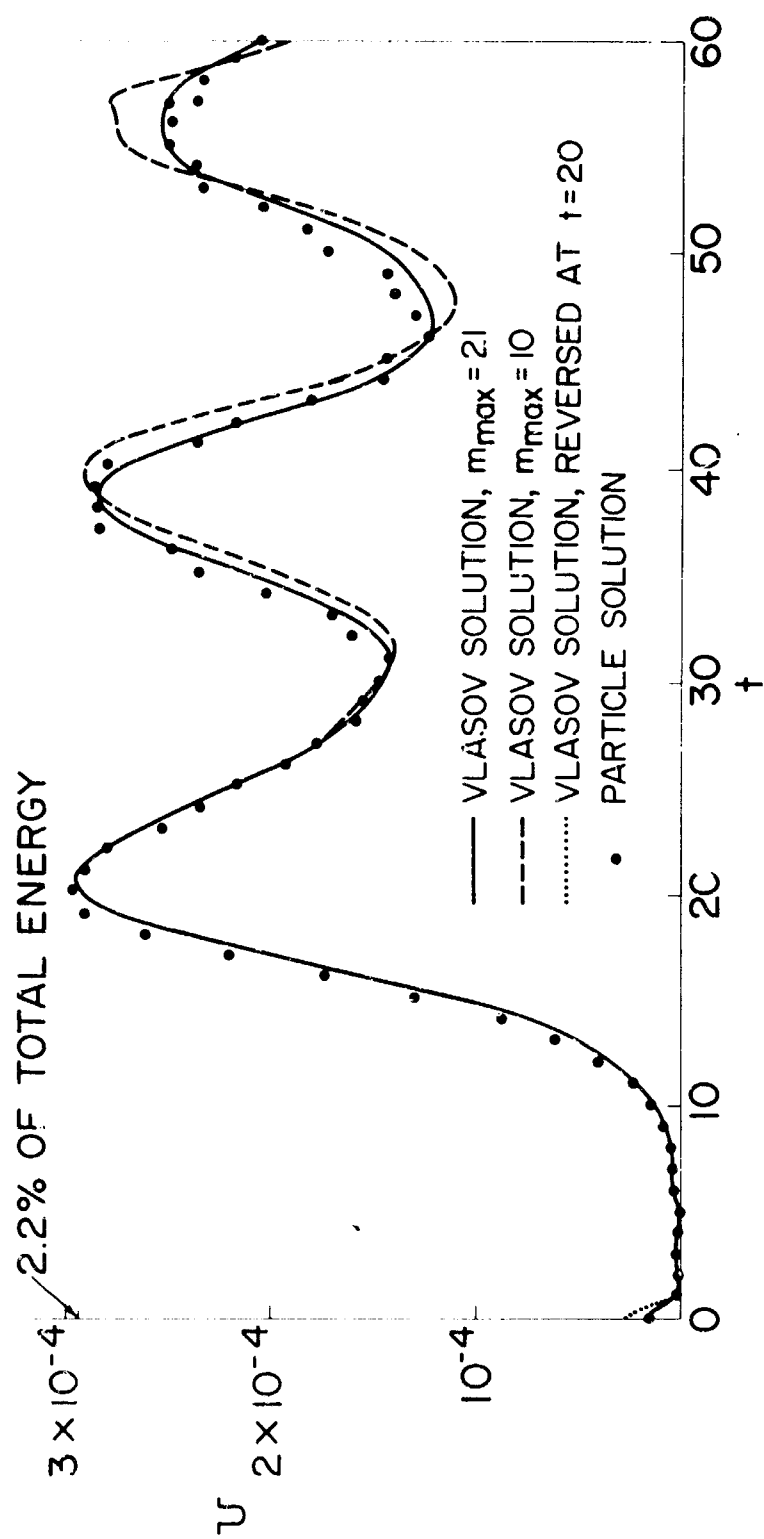Fig. 2 – Determination of initial velocities for a Maxwellian distribution function

29

Fig. 3 - Electrostatic energy for a two-stream instability with equal beams (Case A)
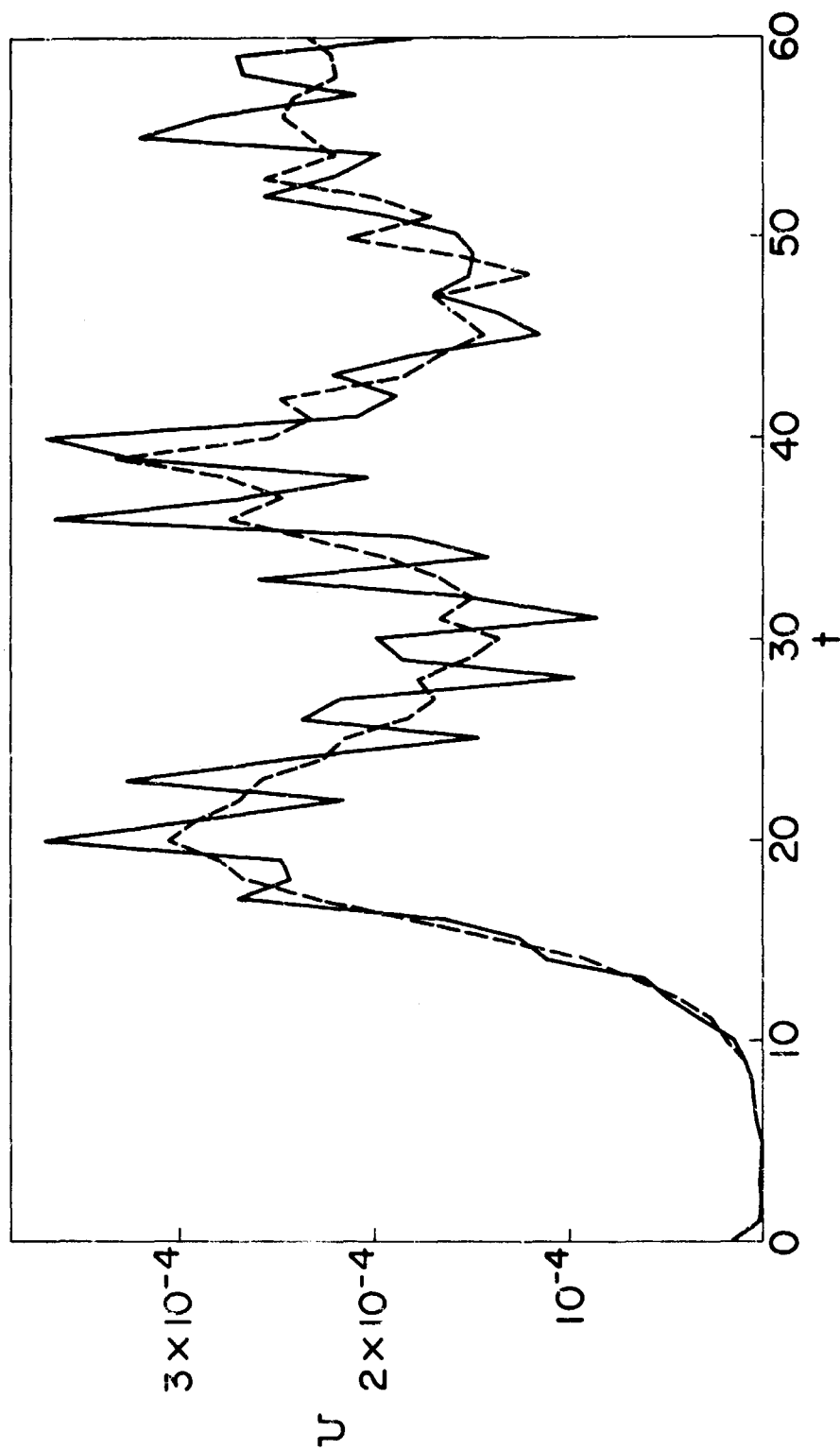
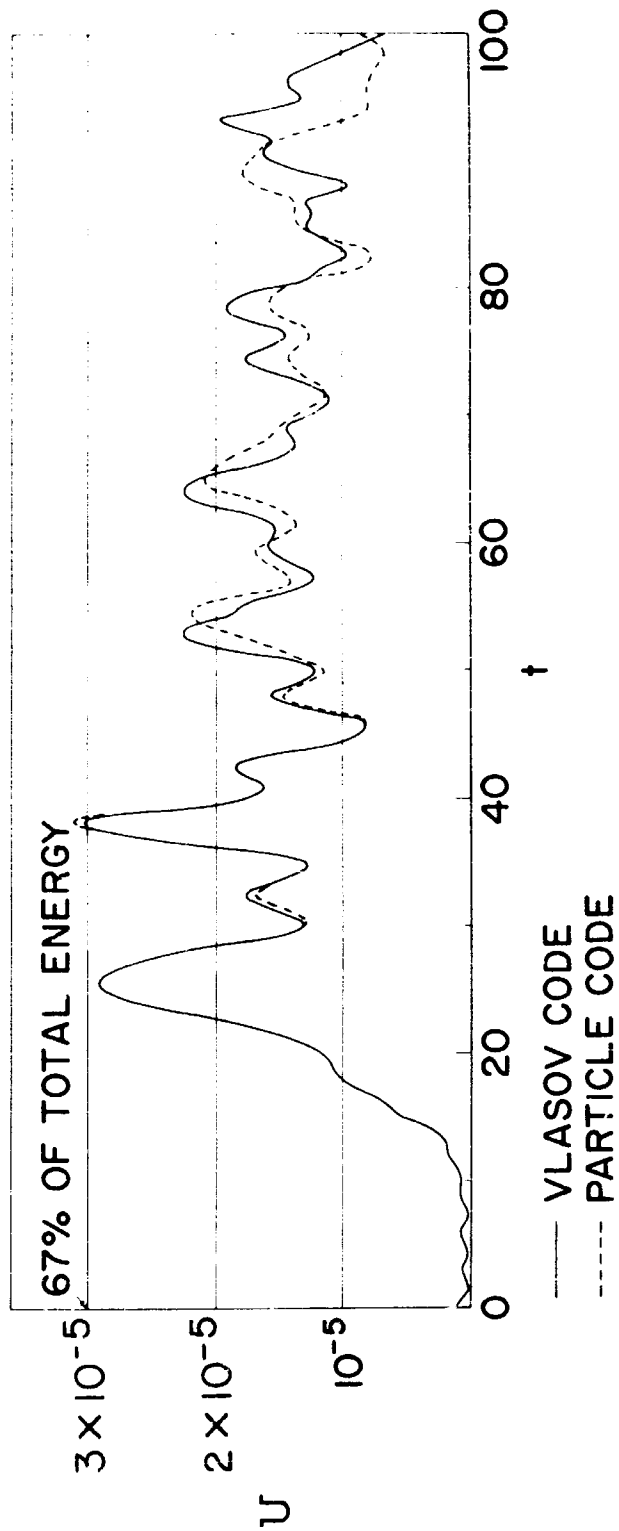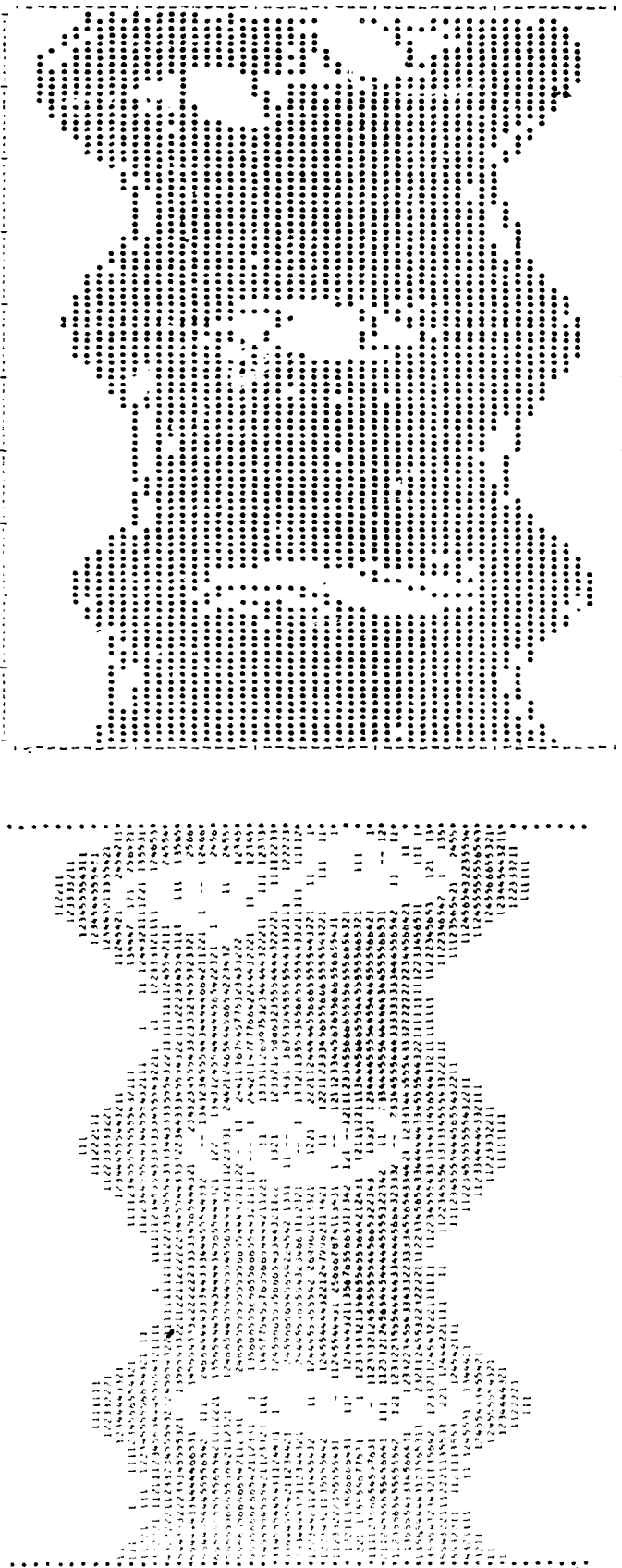Fig. 4 – Effect of discrete beam instability on electrostatic energy for Case A

Fig. 5 – Electrostatic energy for a two-stream instability with equal beams (Case B)

32

PARTICLE CODE
τ = 13

VLASOV CODE
τ = 15.45

Fig. 6 – Density in phase from Vlasov and particle solutions for Case B
at the beginning of instability

33

PARTICLE CODE
t = 23

VLASOV CODE
t = 24.02

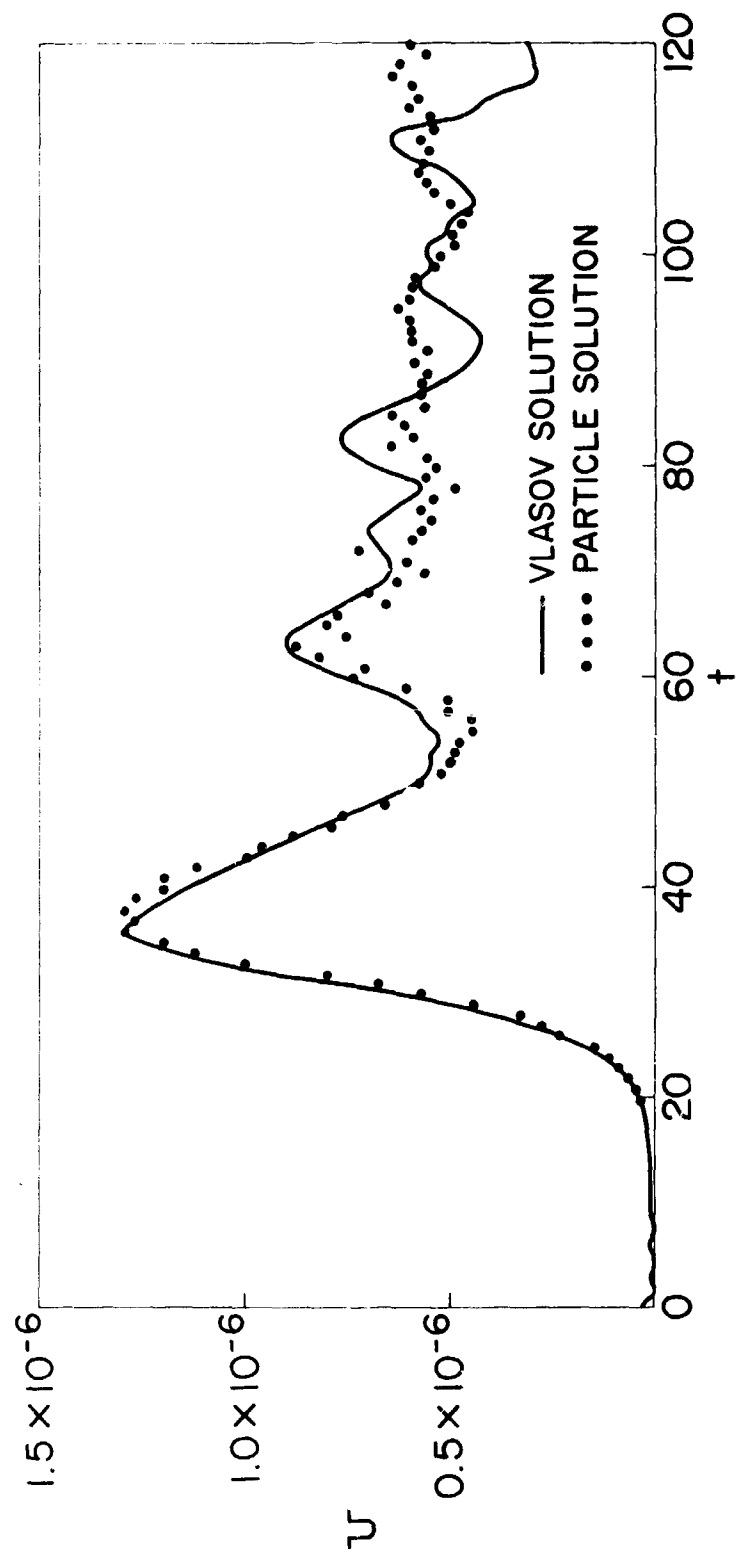Fig. 7 – Density in phase, from Vlasov and particle solutions for Case B near saturation.

34

PARTICLE CODE
t = 93

VLASOV CODE
t = 91.78

Fig. 8 – Density in phase, from Vlasov and particle solutions for Case B near the end of computation.

NOT REPRODUCIBLE

35

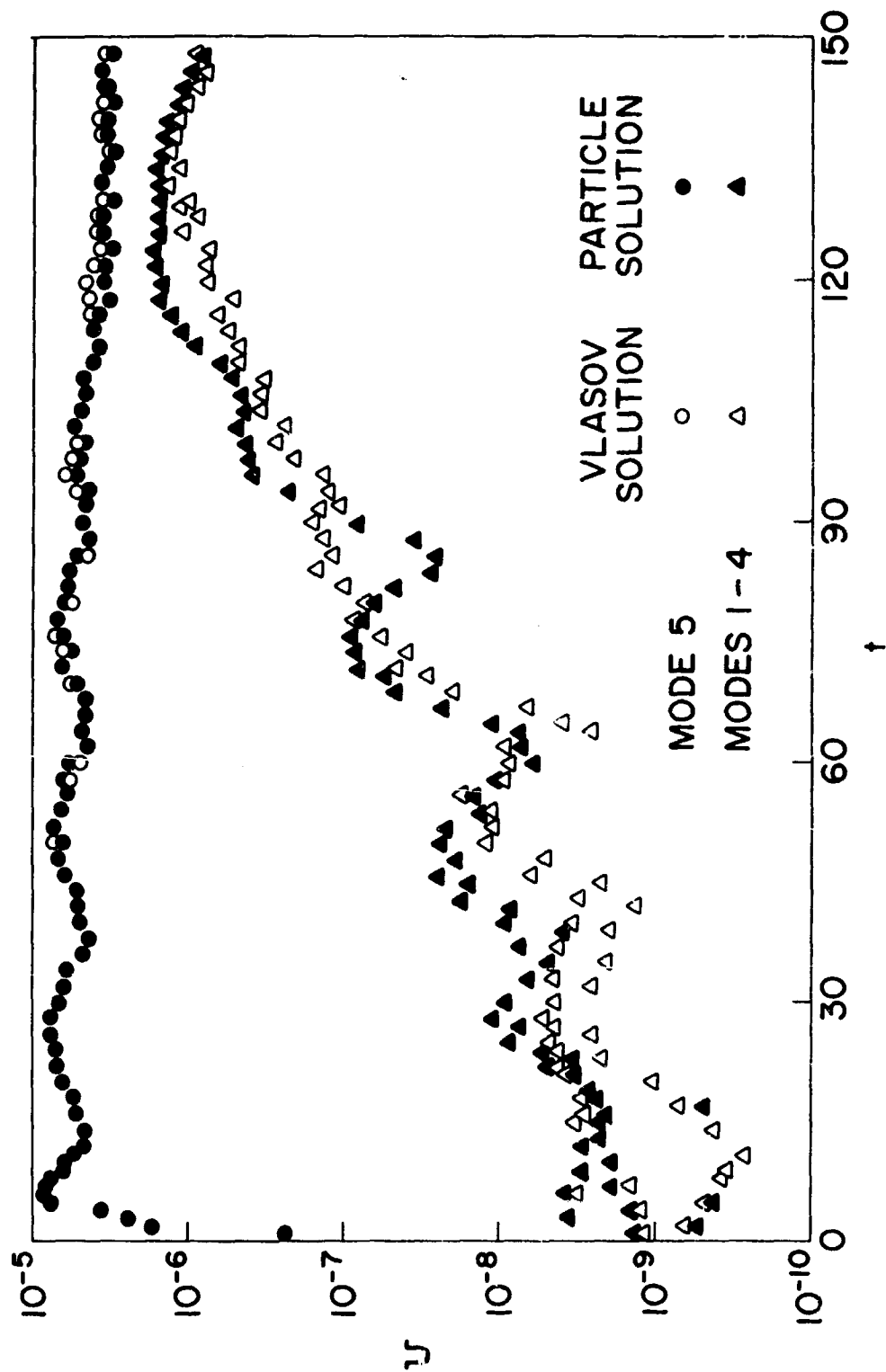Fig. 9 – Electrostatic energy for a two-stream instability with unequal beams (Case C).

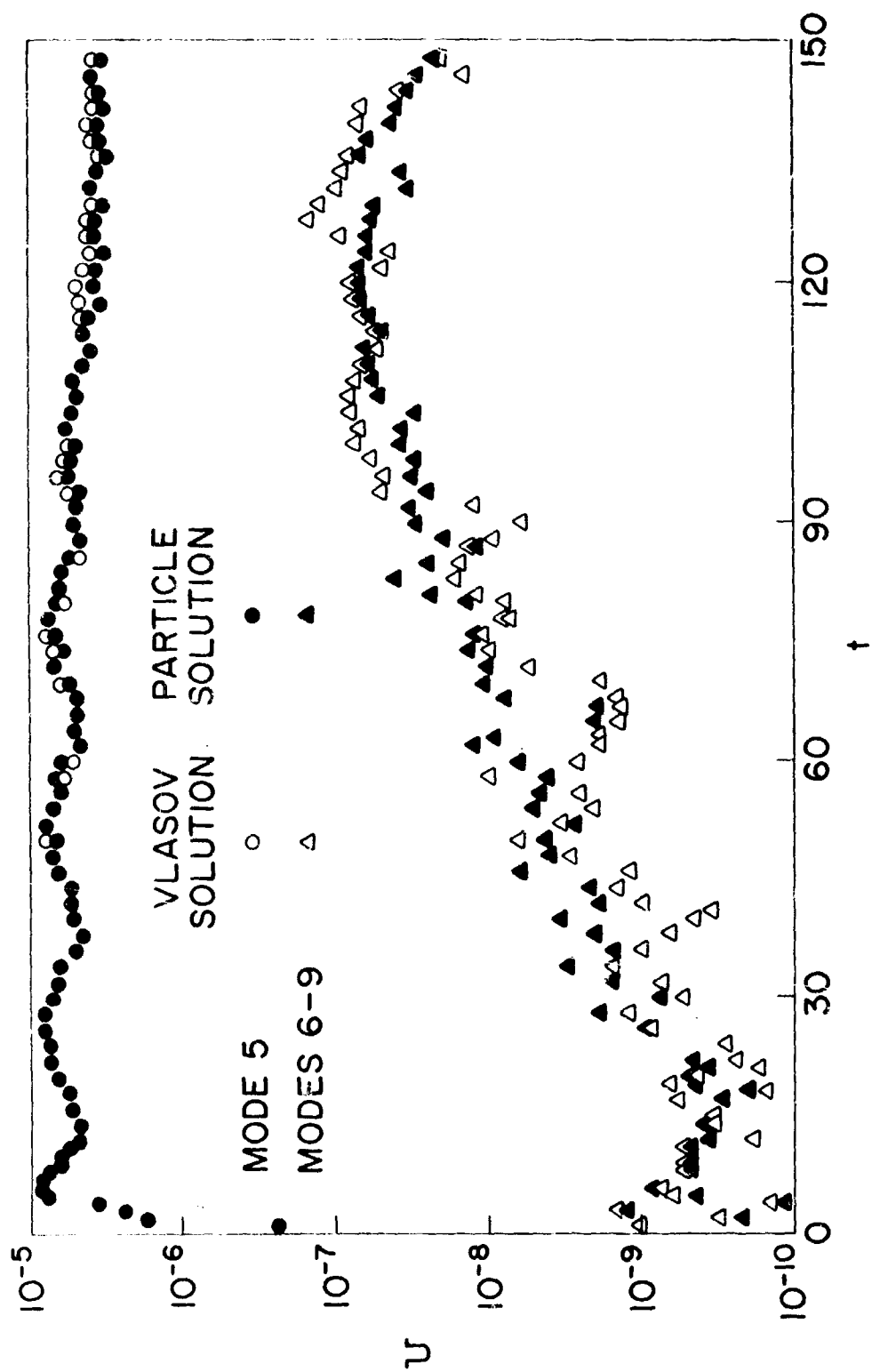Fig. 10 – Electrostatic energy of the main wave and lower sideband. Case D.

Fig. 11 - Electrostatic energy of the main wave and upper sideband, Case D.